A Lysosome-Targeting AIEgen for Autophagy Visualization

*Chris Wai Tung Leung, Zhiming Wang, Engui Zhao, Yuning Hong, Sijie Chen, Ryan Tsz Kin Kwok, Anakin Chun Sing Leung, Rongsen Wen, Bingshi Li, Jacky Wing Yip Lam, and Ben Zhong Tang**

Lysosome is known as the leading player of autophagy.[1] Investigating lysosomal activities is indispensable to in-depth investigation of autophagy, through which cells dissemble unnecessary or dysfunctional cellular components in a regulated manner. Autophagy has become a hot research topic, owing to its close relationship with cancers, aging, longevity, and neurodegenerative diseases, such as Danon disease, Pompe disease, etc.[1–8] Proper autophagic flux is necessary for controlling the health of an individual. Upregulated and downregulated autophagy may lead to the clearance and accumulation of protein aggregates, which may reduce and exaggerate the symptoms of several neurodegenerative diseases, respectively.[9,10] Remarkably, active autophagy is observed in the brain of patients and mouse models of Alzheimer's disease, but autophagy–lysosomal degradation is disrupted, leading to a boost of autophagic compartment accumulation containing amyloid protein and β-amyloid precursor. A typical autophagy process is depicted in **Scheme 1**. A phagophore is formed at the early stages of autophagy, followed by the formation of autophagosome, which is essential to deliver the damaged pieces within the cytoplasm to the lysosomes. The fusion of an autophagosome and lysosome leads to the formation of autolysosome. The encapsulated materials will then be degraded by lysosomal hydrolases. The lysosomes are reformed after the completion of digestion and able to fuse with next autophagosome.[8] In the whole autophagy process, lysosome is the determining subcellular organelle in autophagy execution.

Owing to the close association of lysosome with autophagy, visualizing and tracking lysosomal activities will enrich the insight into the autophagic process. A proper lysosome-targeting probe not only facilitates the investigation of autophagy but also broadens the mechanistic vision of corresponding drugs. With such regard, a variety of lysosome-targeting probes are developed for exploring lysosome-involved cellular activities, among which LysoTracker Red DND-99 (LTR) is a good representative. The emission of LTR is turned on due to the removal of photoinduced electron-transfer (PET) effect by protonation of its weak base unit in the lysosome.[11] Unfortunately, the fluorescence quenching process by PET is not efficient outside the lysosome,[12] thus accurate localization of the lysosome is difficult. On the other hand, the working concentration of LTR is normally low to prevent the aggregation-caused quenching (ACQ) effect. As a result, LTR displays low photostability. Furthermore, LTR exhibits small Stokes shift with absorption and fluorescence maxima at 577 and 590 nm, respectively, thus high-resolution image can only be obtained by choosing appropriate excitation and emission ranges. Besides small organic molecules, lysosome labeling can be achieved by utilizing metal complexes.[11,13–19] However, they may suffer from high background noise, inadequate specificity, lengthy incubation time, and low photostability.

In 2001, a series of luminogens with propeller-shaped conformation were discovered to demonstrate faint emission in solution but fluoresce intensely in their aggregates. We termed the phenomenon as aggregation-induced emission (AIE). Systematic investigations revealed restriction of intramolecular motion (RIM) as the underlying mechanism. AIE luminogens (AIEgens) have been utilized in numerous fluorescence biosensing systems, including organelle targeting, protein probing, DNA differentiation, and so on.[20–30] To obtain higher signal-to-noise ratio, hydrophilic groups, charged moieties or peptide chains can be incorporated into their structures to enhance their water solubility and weaken their emission in aqueous media.[20] In

Dr. C. W. T. Leung, Dr. Z. Wang, Dr. E. Zhao, Dr. S. Chen, Dr. R. T. K. Kwok, A. C. S. Leung, Dr. J. W. Y. Lam, Prof. B. Z. Tang
HKUST Shenzhen Research Institute
Nanshan, Shenzhen 518057, China
E-mail: tangbenz@ust.hk

Dr. C. W. T. Leung, Dr. Z. Wang, Dr. E. Zhao, Dr. S. Chen, Dr. R. T. K. Kwok, A. C. S. Leung, Dr. J. W. Y. Lam, Prof. B. Z. Tang
Department of Chemistry
Hong Kong Branch of Chinese National Engineering Research Center for Tissue Restoration and Reconstruction
Institute for Advanced Study
Division of Biomedical Engineering
Division of Life Science
State Key Laboratory of Molecular Neuroscience and Institute of Molecular Functional Materials
The Hong Kong University of Science & Technology (HKUST)
Clear Water Bay
Kowloon, Hong Kong, China

Dr. Y. Hong
School of Chemistry
The University of Melbourne
Parkville, VIC 3010, Australia

R. Wen, Prof. B. Li
Department of Chemistry and Chemical Engineering
Shenzhen University
Shenzhen 518060, China

Prof. B. Z. Tang
Guangdong Innovative Research Team
SCUT-HKUST Joint Research Laboratory
State Key Laboratory of Luminescent Materials and Devices
South China University of Technology (SCUT)
Guangzhou 510640, China

DOI: 10.1002/adhm.201500674

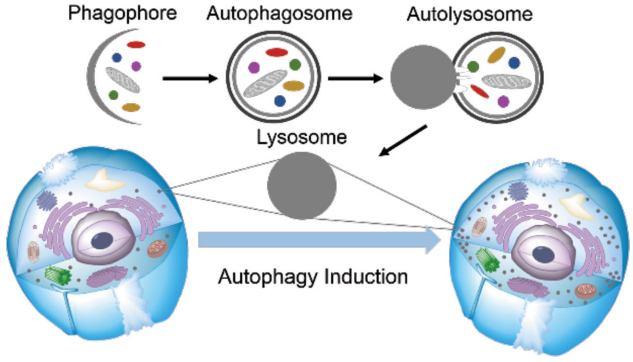

Scheme 1. Schematic presentation of autophagy process induced by rapamycin. The significant increment of number of lysosomes (grey dots) can be observed.

this contribution, we report the design and synthesis of an AIE-active probe with excited-state intramolecular proton-transfer (ESIPT) characteristics, namely AIE-LysoY, and its utility in visualization of the lysosome and lysosome-involved autophagy process (**Scheme 2**).

The synthetic route to AIE-LysoY is shown in Scheme 2. M1 and M2 were prepared by one-step modification of commercially available precursors, which then underwent condensation under mild reaction conditions to yield FAS-Br. AIE-LysoY was obtained by conjugating FAS-Br with morpholine group. The morpholine group with moderate alkalinity is employed for lysosome-targeting.[31] Once entered lysosome, the morpholine will be protonated due to the high acidity of the lysosome, which endows AIE-LysoY with higher hydrophilicity and lysosomal retention.[32] In this way, fluorescence of AIE-LysoY can only be observed in the lysosome area.

AIE-LysoY exhibits an absorption band peaked at 390 nm in THF (Figure S1, Supporting Information). It emits faintly when it is dissolved in THF with a small emission band centered at 565 nm. With an increase in water fraction of the THF/water mixtures, AIE-LysoY becomes highly emissive (**Figure 1**B), demonstrating a phenomenon of AIE. The AIE effect of AIE-LysoY can be rationalized by the activation of RIM and ESIPT upon formation of nanoaggregates. In pure THF solution, AIE-LysoY can undergo dynamic intramolecular motions, thus excitons nonradiatively decay in these solutions. In solvent mixture with low solvating power, AIE-LysoY form nanoaggregates, and thus its intramolecular motion is prohibited. As a result, the excitons of AIE-LysoY decay through the radiative pathway of fluorescence and its emission is enhanced.

AIE-LysoY also possesses the characteristics of ESIPT. It demonstrates two kinds of emission (Scheme S1, Supporting Information). In aprotic solvent, intramolecular hydrogen bond exists, thus it exhibits keto emission with longer wavelength, while it displays the enol emission with shorter wavelength in protic solvent due to the breakage of such intramolecular hydrogen bond (Figure S2, Supporting Information). Besides, addition of organic acid can also break the intramolecular hydrogen bond and lead to decreased keto emission intensity. To demonstrate this, a strong organic acid, trifluoroacetic acid (TFA), with a p*K*a of about –0.3, is added into the aggregate suspension (THF/water, 1:99) of AIE-LysoY. The emission of AIE-LysoY at 565 nm decreases dramatically when the TFA fraction is increased from 1% to 5%. When the TFA fraction reaches 10%, AIE-LysoY becomes completely nonemissive (**Figure 2**) due to the protonation of the central nitrogen and destroy of the ESIPT emission.

Before employing AIE-LysoY to visualize the lysosome, we first conducted 3-(4,5-dimethyl-2-thiazolyl)-2,5-diphenyltetrazolium bromide (MTT) cell proliferation assay to evaluate its cytotoxicity. Even after incubation with 15×10^{-6} M of AIE-LysoY for 24 h, the viability of HeLa cell remains higher than 80% (Figure S3, Supporting Information), indicating that AIE-LysoY exerts little interference on cell growth. The good biocompatibility of AIE-LysoY enables its application as a fluorescent tracer to follow the autophagic process of lysosome.

Then, AIE-LysoY was applied to imaging of the lysosome and its lysosome-targeting performance was assessed by fluorescence microscope. HeLa cells were stained with 10×10^{-6} M of AIE-LysoY for 10 min, followed by washing away the unbounded molecules of AIE-LysoY and incubation with 50×10^{-9} M of LTR for 30 min. As shown in **Figure 3**A, AIE-LysoY selectively accumulates in the punctate lysosomes and endows them with yellow emission, which can be clearly distinguished from the background. Besides, the fluorescence of

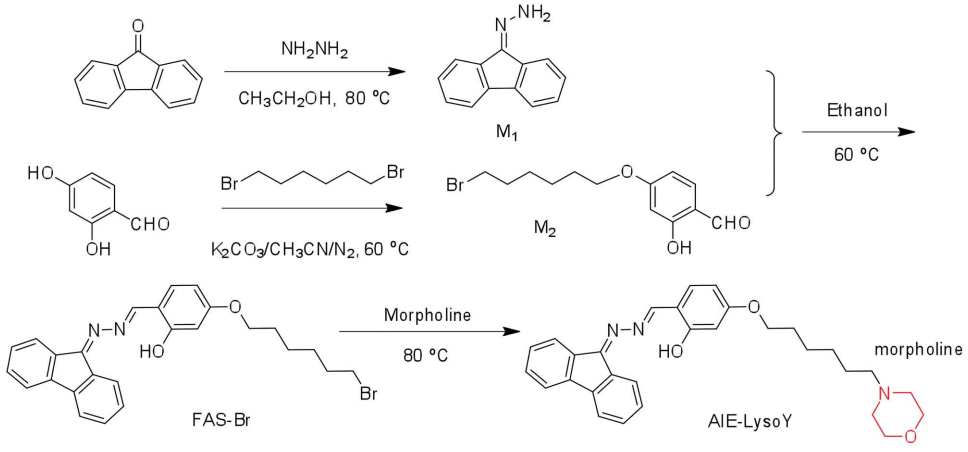

Scheme 2. Sythetic route of AIE-LysoY.

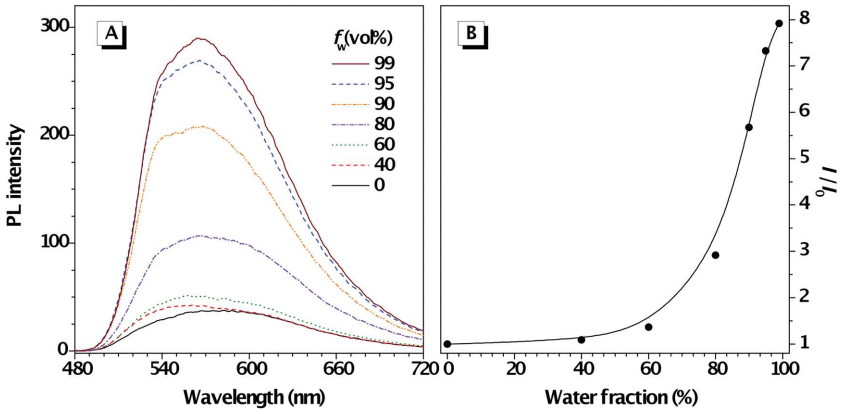

Figure 1. A) PL spectra of AIE-LysoY in THF/water mixtures with different water fractions (f_w). B) Plot of I/I_0 versus the composition of the THF/water mixture of AIE-LysoY. Concentration = 10×10^{-6} M; I_0 = PL intensity in pure THF solution; $\lambda_{ex/em}$ = 390/565 nm.

AIE-LysoY overlaps perfectly with that of LTR, indicating the lysosome targeting of AIE-LysoY. Quantitative analysis of the degree of overlapping of these two fluorescence signals by Pearson's coefficient (R_r), which depicts the degree of linear dependence between two variables, gives an overlapping coefficient of 0.90 (Figure 3C). The high R_r value proves that AIE-LysoY is a lysosome-selective probe. In addition, AIE-LysoY shows a higher contrast than LTR even after shorter incubation time, which can be ascribed to the bright emission and high selectivity of AIE-LysoY. Interestingly, if HeLa cells are stained with LTR in the first place and then AIE-LysoY, the latter still demonstrates higher contrast than the former (Figure S4, Supporting Information). These results suggest that AIE-LysoY may compete with LTR to bind to lysosome, but AIE-LysoY possesses higher affinity to lysosome than LTR. Additionally, AIE-LysoY also demonstrates advantageous attribute of variable staining time. Changing the staining time from 10 to 60 min, the specificity to lysosome and emission contrast is well retained (Figure S5, Supporting Information).

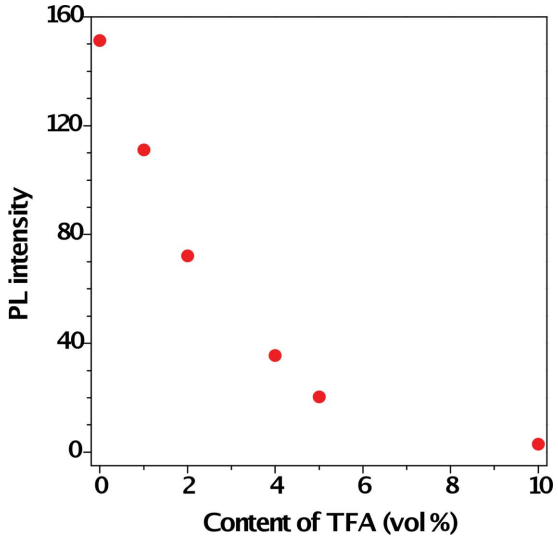

Figure 2. PL intensities in of AIE-LysoY THF/water (1:99 v/v) mixtures with different TFA fractions. Concentration = 10×10^{-6} M; $\lambda_{ex/em}$ = 390/565 nm.

Compared with LTR, the working concentration of AIE-LysoY is much higher. One may think that LTR is more sensitive than AIE-LysoY and thus more advantageous, but it is not true. As mentioned previously, LTR can only be used at low concentration to avoid the ACQ effect. At such low working concentration, the fluorescent probes molecularly disperse in the organelle and can be easily photo-oxidized by continuous excitation light irradiation, resulting in the low photostability of these probes. For AIE-LysoY, its emission is brightened by aggregation, thus can be used at high concentrations to image the lysosome with high brightness and photostability. In order to evaluate the photostability of AIE-LysoY, confocal microscope (Zeiss laser scanning confocal microscope LSM7 DUO) was applied to continuously scan cells stained by AIE-LysoY. The photostability of LTR was also measured for comparison. The power of excitation light (405 nm for AIE-LysoY and 561 nm for LTR) were unified by using a power meter. After continuous scanning for 50 times with total irradiation time of ≈6 min, the fluorescence signal from AIE-LysoY almost remain unchanged, indicating its excellent photostability (**Figure 4**, red line; video 1, Supporting Information). In contrast, the fluorescence intensity from LTR drops to lower than 50% of its initial value after only 25 scans (Figure 4, blue line; video 2, Supporting Information). The slightly fluctuation of fluorescence signal can be ascribed to the dynamic movement of the lysosome in living cells. The excellent photostability of AIE-LysoY may stem from its nanoparticles nature in lysosome imaging, which can protect the chromophore inside the particles from being photo-oxidized. In this way, the fluorescence of AIE-LysoY can remain after long-time irradiation. The good photostability of AIE-LysoY enables its potential in long-term following the biological processes of lysosome.

To build up a more general strategy for designing lysosome-specific bioprobe, molecular engineering approach was employed. The precursor of AIE-LysoY, FAS–Br, and two morpholine-functionalized AIEgens, TPE-2Mor and Nred-mor (Scheme S2–S4, Supporting Information), were prepared and applied to cell imaging. FAS–Br lights up intracellular lipid droplets and the reticulum structures of the mitochondria in HeLa cells (Figure S6, Supporting Information) rather than the lysosome, which suggests the necessity of morpholine for locating the acidic lysosome. However, bearing morpholine group does not guarantee lysosome selectivity. Both TPE-2Mor

Figure 3. Fluorescence images of HeLa cells stained with A) AIE-LysoY (10×10^{-6} M) for 10 min and B) LysoTracker red (LTR, 50×10^{-9} M) for 30 min. C) Merged image of A) and B). λ_{ex} = 400–440 nm (for AIE-LysoY) and 540–580 nm (for LTR).

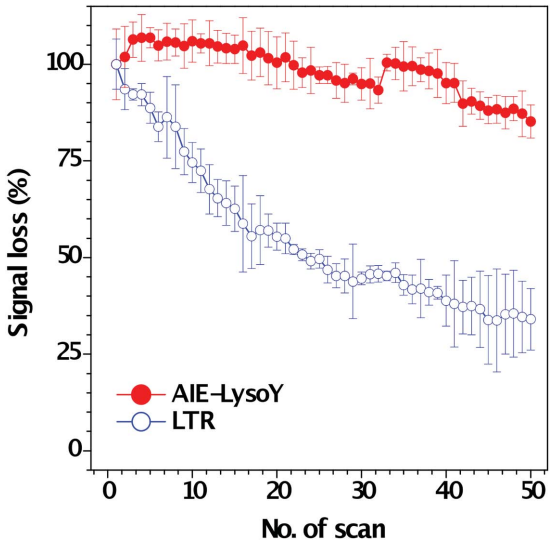

Figure 4. Signal loss (%) of fluorescence emission of AIE-LysoY (solid circle) and LTR (open circle) with increasing number of scans. λ_{ex} = 405 nm (for AIE-LysoY) and 561 nm (for LTR); λ_{em} = 468–696 nm (for AIE-LysoY) and 573–696 nm (for LTR); irradiation time: 7.75 s per scan.

and Nred-mor contain morpholine group, but none of them can selectively light up the lysosome. TPE-2Mor stains all the hydrophobic region, while Nred-mor selectively accumulates in the mitochondria (Figures S7 and S8, Supporting Information). TPE-2Mor contains a hydrophobic tetraphenylethene (TPE) core and Nred-mor carries a charged pyridinium moiety. The hydrophobic interaction of TPE and the electrostatic interaction of positively charged pyridinium with other cellular organelles may compete with the driving force from morpholine and thus decrease or destroy the lysosome selectivity. Therefore, accurate lysosome targeting should go with the manipulation of hydrophobicity and polarity cautiously.

Mammalian target of rapamycin (mTOR) has been identified as the suppressant of autophagy. Rapamycin, a lipophilic macrolide antibiotic (Scheme S5, Supporting Information), can bind to mTOR and enhance autophagy and is thus widely used for autophagy induction. Treatment with rapamycin has been demonstrated to prolong the survival of prion protein infected mice by activating autophagy and prion protein degradation.[9] During rapamycin treatment, there is an increase in the number, size, and acidity of the lysosome. By employing AIE-LysoY with high lysosome targetability and excellent photostability as fluorescent visualizer, the autophagy process can be tracked in long term, which will provide more insight into the cellular activities. To demonstrate this feasibility, HeLa cells were incubated with 10×10^{-6} M of AIE-LysoY for 10 min and then treated with rapamycin for different periods of time, followed by observation under fluorescence microscope. As shown in **Figure 5**A–E, the lysosome can be clearly visualized under the fluorescence microscope. During autophagy process, the lysosome will increase in amount and they will fuse with autophagosome to form autolysosome. This is indeed the case. The amount of yellow spots, which corresponds to the number of lysosome, are increased with prolonged rapamycin treatment. If we enlarge the image in Figure 5E, the lysosome can be visualized with excellent resolution and contrast (Figure 5F). Notably, the newly formed lysosomes were lit up even when the excessive AIE-LysoY was removed prior to rapamycin treatment. The result strengthened the occurrence of the fusion between the autophagic compartment and primitive lysosome during autophagy.[3] In addition, LTR provided similar fluorescence images and showed good overlapping with AIE-LysoY in rapamycin-treated HeLa cells (Figures S9 and S10, Supporting Information). However, LTR should be co-incubated with rapamycin, otherwise its emission will be greatly diminished when excessive LTR is washed away beforehand (Figure S11, Supporting Information). By virtue of its high selectivity towards the lysosome and excellent photostability, AIE-LysoY is an excellent candidate as lysosome selective bioprobe for investigating autophagy process.

In conclusion, an AIE-active lysosome-specific probe with ESIPT characteristics, namely AIE-LysoY, was designed and developed. Guided by its morpholine functionality, AIE-LysoY selectively accumulates in and lights up the lysosome of cells. Thanks to the collective effect of AIE and ESIPT properties,

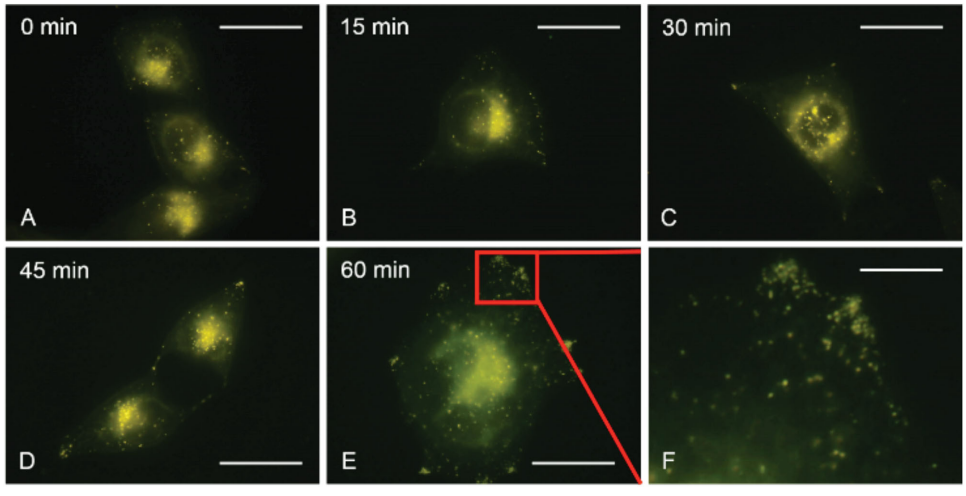

Figure 5. A–E) Fluorescence images of AIE-LysoY (10×10^{-6} M) stained HeLa cells before and after rapamycin treatment (50 μg mL^{-1}) for different periods of time. F) Enlarged region of interest of panel E. Scale bar: A–E) 30 μm, F) 10 μm. λ_{ex} = 400–440 nm.

AIE-LysoY can visualize the lysosome in HeLa cells with superior resolution and contrast. It also enjoys the advantages of large Stokes shift, simple operation, varied incubation concentration, and time, excellent photostability and high affinity towards the lysosome, which enables it to locate the lysosomes accurately and provide more insight on lysosomal-related intracellular activities such as autophagy.

Supporting Information

Supporting Information is available from the Wiley Online Library or from the author.

Acknowledgements

C.W.T.L. and Z.W. contributed equally to this work. This work was partially supported by the National Basic Research Program of China (973 Program, 2013CB834701), the University Grants Committee of Hong Kong (AoE/P-03/08), the Research Grants Council of Hong Kong (604913, 16301614 and N_HKUST604/14), the Innovation and Technology Commission (ITC-CNERC14S01), the Science and Technology Plan of Shenzhen (JCYJ20140425170011516) and the Natural Science Fund of Guangdong Province (2014A030313659). The authors thank the support of the Guangdong Innovative Research Team Program (201101C0105067115).

Received: August 25, 2015
Revised: November 2, 2015
Published online: December 20, 2015

[1] S. Castro-Obregon, *Nat. Educ.* **2010**, *3*, 49.
[2] H. Nakatogawa, K. Suzuki, Y. Kamada, Y. Ohsumi, *Nat. Rev. Mol. Cell Biol.* **2009**, *10*, 458.
[3] E.-L. Eskelinen, P. Saftig, *Biochim. Biophys. Acta Rev. Cancer* **2009**, *1793*, 664.
[4] N. Mizushima, *Genes Dev.* **2007**, *21*, 2861.
[5] M. C. Malicdan, S. Noguchi, I. Noaka, P. Saftig, I. Nishino, *Neuromuscular Disord.* **2008**, *18*, 521.
[6] A. P. Lieberman, R. Puertollano, N. Raben, S. Slaugenhaupt, S. U. Walkley, A. Ballabio, *Autophagy* **2012**, *8*, 719.
[7] S. T. Stern, P. P. Adiseshaiah, R. M. Crist, *Part. Fibre Toxicol.* **2012**, *9*, 20.
[8] M. E. Orr, S. Oddo, *Alzheimers Res. Ther.* **2013**, *5*, 53.
[9] A. Heiseke, Y. Aguib, C. Riemer, M. Baier, H. M. Schätzl, *J. Neurochem.* **2009**, *109*, 25.
[10] C. J. Cortes, K. Qin, J. Cook, A. Solanki, J. A. Mastrianni, *J. Neurosci.* **2012**, *32*, 12396.
[11] S.-L. Shen, X.-P. Chen, X.-F. Zhang, J.-Y. Miao, B.-X. Zhao, *J. Mater. Chem. B* **2015**, *3*, 919.
[12] L. Z. Chen, J. Li, Z. Z. Liu, Z. Ma, W. Zhang, L. P. Du, W. F. Xu, H. Fang, M. Y. Li, *RSC Adv.* **2013**, *3*, 13412.
[13] L. He, C.-P. Tan, R.-R. Ye, Y.-Z. Zhao, Y.-H. Liu, Q. Zhao, L.-N. Ji, Z.-W. Mao, *Angew. Chem. Int. Ed.* **2014**, *53*, 12137.
[14] M. Gao, Q. Hu, G. Feng, B. Z. Tang, B. Liu, *J. Mater. Chem. B* **2014**, *2*, 3438.
[15] X. Wang, D. M. Nguyen, C. O. Yanez, L. Rodriguez, H.-Y. Ahn, M. V. Bondar, K. D. Belfield, *J. Am. Chem. Soc.* **2010**, *132*, 12237.
[16] H. Wang, Y. Wu, Y. Shi, P. Tao, X. Fan, X. Su, G.-C. Kuang, *Chem. Eur. J.* **2015**, *21*, 3219.
[17] J. H. Han, S. K. Park, C. S. Lim, M. K. Park, H. J. Kim, H. M. Kim, B. R. Cho, *Chem. Eur. J.* **2012**, *18*, 15246.
[18] W. Yang, P. S. Chan, M. S. Chan, K. F. Li, P. K. Lo, N. K. Mak, K. W. Cheah, M. S. Wong, *Chem. Commun.* **2013**, *49*, 3428.
[19] I. Takashima, R. Kawagoe, I. Hamachi, A. Ojida, *Chem. Eur. J.* **2015**, *21*, 2038.
[20] D. Ding, K. Li, B. Liu, B. Z. Tang, *Acc. Chem. Res.* **2013**, *46*, 2441.
[21] R. T. K. Kwok, C. W. T. Leung, J. W. Y. Lam, B. Z. Tang, *Chem. Soc. Rev.* **2015**, *44*, 4228.
[22] J. Mei, Y. Hong, J. W. Y. Lam, A. Qin, Y. Tang, B. Z. Tang, *Adv. Mater.* **2014**, *26*, 5429.
[23] M. Wang, D. Zhang, G. Zhang, Y. Tang, S. Wang, D. Zhu, *Anal. Chem.* **2008**, *80*, 6443.
[24] J. Qian, Z. Zhu, C. W. T. Leung, W. Xi, L. Su, G. Chen, A. Qin, B. Z. Tang, S. He, *Biomed. Opt. Express* **2015**, *6*, 1477.
[25] H. Cheng, W. Qin, Z. F. Zhu, J. Qian, A. Qin, B. Z. Tang, S. He, *Prog. Electromagn. Res.* **2013**, *140*, 313.
[26] F. Hu, Y. Huang, G. Zhang, R. Zhao, H. Yang, D. Zhang, *Anal. Chem.* **2015**, *86*, 7987.
[27] X. Cheng, H. Jia, J. Feng, J. Qin, Z. Li, *Sens. Actuators, B* **2014**, *199*, 54.
[28] X. Xue, Y. Zhao, L. Dai, X. Zhang, X. Hao, C. Zhang, S. Huo, J. Liu, C. Liu, A. Kumar, W.-Q. Chen, G. Zou, X.-J. Liang, *Adv. Mater.* **2014**, *26*, 712.
[29] Y. Zhang, K. Chang, B. Xu, J. Chen, L. Yan, S. Ma, C. Wu, W. Tian, *RSC Adv.* **2015**, *5*, 36837.
[30] K. Wang, X. Zhang, X. Zhang, B. Yang, Z. Li, Q. Zhang, Z. Huang, Y. Wei, *Polym. Chem.* **2015**, *6*, 1360.
[31] L. Wang, Y. Xiao, W. Tian, L. Deng, *J. Am. Chem. Soc.* **2013**, *135*, 2903.
[32] H. Yu, Y. Xiao, L. Jin, *J. Am. Chem. Soc.* **2012**, *134*, 17486.